Geomechanics and Engineering, *Vol. 23, No. 5 (2020) 431-439*
DOI: https://doi.org/10.12989/gae.2020.23.5.431

A simplified directly determination of soil-water retention curve variables

Geng Niu[1,2a], Longtan Shao*[1,2] and Xiaoxia Guo[1,2b]

[1]*State Key Laboratory of Structural Analysis for Industrial Equipment, Dalian University of Technology, 116024 Dalian, Liaoning Province, China*
[2]*Department of Engineering Mechanics, Dalian University of Technology, 116024 Dalian, Liaoning Province, China*

(Received July 2, 2020, Revised November 17, 2020, Accepted November 21, 2020)

Abstract. Soil-water retention curve (SWRC) contains key information for the application of unsaturated soil mechanics principles to engineering practice. The SWRC variables are commonly used to describe the hydro-mechanics of soils. Generally, these parameters are determined using the graphical method which can be time consuming. The SWRC is highly dependent on the pore size distribution (PSD). Theoretically, the PSD obtained by mercury intrusion porosimetry test can be used to determine some SWRC variables. Moreover, the relationship between SWRC and shrinkage curve has been investigated. A new method to determine total SWRC variables directly without curve-fitting procedure is proposed. Substituting the variables into linear SWRC equations construct SWRC. A good agreement was obtained between predicted and measured SWRCs, indicating the validity of the proposed method for unimodal SWRC.

Keywords: soil water retention curve; pore size distribution; air-entry value; residual value; soil shrinkage curve

1. Introduction

Soil-water retention curve (SWRC), which defines the relationship between matric suction and water amount in the soil, contains key information for the application of unsaturated soil mechanics principles (Fredlund 2019). SWRC can be employed to describe the permeability coefficient (Rahimi *et al.* 2015, Oren *et al.* 2018), shear strength (Gao *et al.* 2020, Zhou *et al.* 2016), deformation (Zhang *et al.* 2012), evaporation behavior (An *et al.* 2018), swelling behavior (Darde *et al.* 2020) and constitutive modeling of unsaturated soil (Sheng *et al.* 2004, Pereira *et al.* 2005). Generally, water retention behavior for general soils is highly dependent on the pore size in a low suction range where water-soil interactions are mainly governed by capillarity effect (Fredlund *et al.* 2011). Therefore, many researchers (Aung *et al.* 2001, Romero 1999) used pore size distribution (PSD) to calculate SWRC indirectly. However, the calculated SWRC does not include the volume change effect and there is significant difference between measured and calculated SWRCs (Simms and Yanful 2002, Salager *et al.* 2013). Thus, the shrinkage behavior should be kept in mind in predicting SWRC from PSD. Soil-shrinkage curve (SSC), describing the relationship between volume change and water content, gives an insight into soil-water interaction and the deformation behavior. In subsequent years, the shrinkage behavior of soil has been shown to influence hydro-mechanical behaviors and has a close relationship with SWRC (Chin *et al.* 2010, An *et al.* 2017).

Some SWRC variables such as air entry value (AEV), the water content at AEV, the slope at the inflection point, residual value (RV) and the water content at RV are the key points in SWRC. These key variables are commonly used to describe the water retention behavior (Zhai and Rahardjo 2012) and other associated properties (Fredlund 2019). As a simplified method, SWRC can be described as three and five linear segments for unimodal and bimodal SWRC respectively (Pham *et al.* 2016, Niu *et al.* 2020). The key problem in this method is tightly linked to the determination of these SWRC variables. Generally, the conventional graphical method was used to determine these variable: draw the tangent line through the inflection point, followed by a horizontal line through the initial point and another tangent line through the point where the curve starts to drop linearly in the high suction range. Finally the intersections of these tangent lines indicate AEV and the residual state. In the past few decades, various methods were used to determine directly SWRC variables, such as grain-size distribution (GSD) (Chin *et al.* 2010, Russell 2014), the fractal model (Xu 2004) and PSD (Niu *et al.* 2020). However, these parameters are generally determined using the graphical method which can be time consuming.

In order to determine SWRC variables directly without prior measured SWRC data, an insight into the relationship between SWRC, PSD and SSC is investigated in this study. Based on the investigation of the interrelationship between SWRC and PSD, a method to determine AEV, RV and the gravimetric water contents at RV from PSD is proposed. And the gravimetric water content at AEV can be determined by SSC. Then substituting the SWRC variables into liner SWRC equations can construct SWRC.

2. Determining SWRC from PSD considering shrinkage

*Corresponding author, Professor
E-mail: shaolt@dlut.edu.cn, shaolt@hotmail.com
[a]Ph.D.
E-mail: niugeng@mail.dlut.edu.cn
[b]Professor
E-mail: hanyuer@dlut.edu.cn

ISSN: 2005-307X (Print), 2092-6219 (Online)

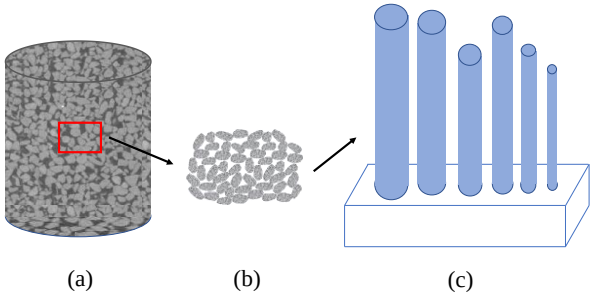

Fig. 1 Conceptual sketch of a bundle of cylindrical capillaries in SWRC and MIP test: (a) soil sample, (b) soil pores and (c) bundle of cylindrical capillaries

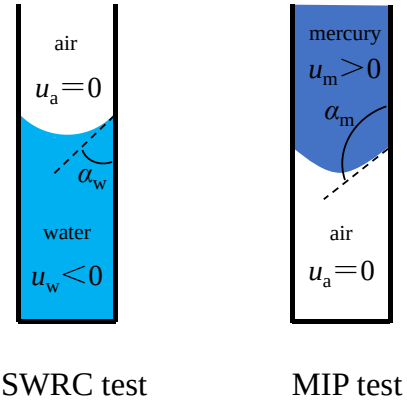

Fig. 2 Schematic diagram of air-water interface and mercury-air interface

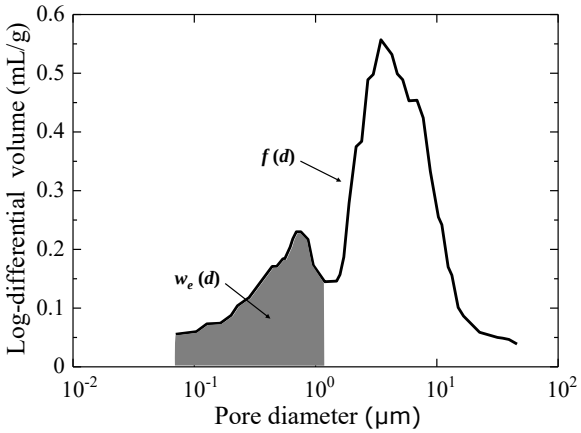

Fig. 3 The effective degree of saturation calculated by PSD of MIP test

As the pore structure in soil is complex, it's difficulty to use test technologies to evaluate the geometrical shape and size of pores in soil. Thus, it is general to consider soil pores as a bunch of cylindrical capillaries of different diameter (Or and Tuller 2002). Fig. 1 shows the conceptual sketch of a bundle of cylindrical capillaries (BCC) describing soil pores.

Fig. 2 shows the schematic diagram of air-water interface and air-mercury interface. The interface medium in MIP test is mercury (non-wetting liquid), while the interface medium in SWRC test is water (wetting liquid). Therefore, the mercury intrusion process in MIP test can describe the drainage process of water in SWRC test (Wang *et al.* 2016). In this regard, the mercury (a non-wetting fluid) intrusion process can be used to extrapolate SWRC for drying.

Matric suction mainly governed by the capillary force is dependent on pore size in a certain range (Sun *et al.* 2017). Early conceptual models for the water distribution in soil pores are based on BCC conceptualizing the pores in soils as an assembly of parallel capillary tubes to represent the pore geometry (Or and Tuller 2002), as illustrated in Fig. 1(c).

According to the Young-Laplace equation, when given a certain pore diameter, there will be a suction accordingly:

$$s = \frac{4T_w cos\alpha_w}{d} \tag{1}$$

where s is general suction; T_w is the water-gas interfacial tension at 20°C (treated as 0.072 N/m); α_w is the water-soil contact angle (treated as 0); d is pore diameter.

As illustrated in Fig. 2(b), the principle of MIP test is that the mercury (non-invasive liquid) will entry the void pore of soil step by step with pressure increasing. The relationship between the pore diameter and applied mercury pressure can be shown as follows:

$$p(d) = \frac{4T_m cos\alpha_m}{d} \tag{2}$$

where p(d) is the pressure applied in MIP; T_m is the mercury surface tensions (treated as 0.485 N/m); α_m is the mercury-soil contact angle (treated as 130°); d is pore diameter.

There is a specific relationship between the pressure applied in MIP test and the suction in SWRC test based on Eqs. (1) and (2):

$$s = 0.196 * p(d) \tag{3}$$

As shown in Fig. 2, the principles of MIP test and SWRC are highly dependent on the pore size. And the cumulative intruded volume of mercury should be equal to the air intrusion volume in SWRC tests. When given a suction, the larger pores than the pore corresponding to the suction are empty, whereas smaller pores are filled completely with water (Sun *et al.* 2016). As illustrated in Fig. 3, the effective gravimetric water content can be calculated:

$$w_e(d) = \int_{d_{min}}^{d} f(d)\,\mathrm{d}d \tag{4}$$

where $w_e(d)$ is the effective gravimetric water content; d is the pore diameter; d_{min} is the smallest effective pore diameter in MIP test; $f(d)$ is the PSD as a function of pore diameter.

The residual gravimetric water content is defined as:

$$w_r = w_s - \int_{d_{min}}^{d_{max}} f(d)\,\mathrm{d}d \tag{5}$$

where w_r is the residual gravimetric water content; w_s is the water content of saturated sample; d_{max} is the largest effective pore diameter in MIP test.

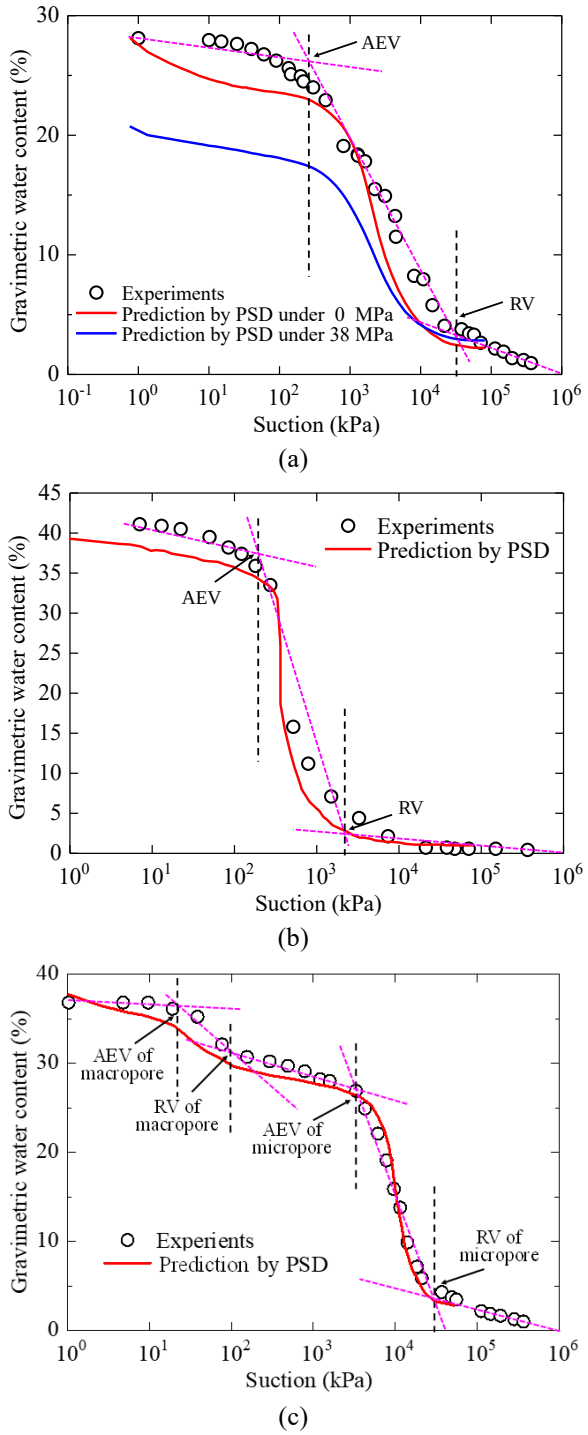

Fig. 4 Measured and predicted SWRC by PSD: (a) for undisturbed complete-intense weathering mudstone (modified from Niu *et al.* 2019), (b) for reconstituted Pearl clay (modified from Gao and Sun 2017) and (c) for compacted lateritic clay (modified from Sun *et al.* 2016)

Then the global gravimetric water content can be calculated as follow:

$$w = w_e(d) + w_r \quad (6)$$

Although PSD obtained by MIP test can be used to predict the SWRC (Sun *et al.* 2016), the agreement between the calculated and measured curve is not very good, especially in lower suction range (Sun *et al.* 2016, Niu *et al.* 2020). The PSDs at different suctions in SWRC test are different. In this case, the deformation can cause the error between the experimental and predicted curve, specifically for deformable clays.

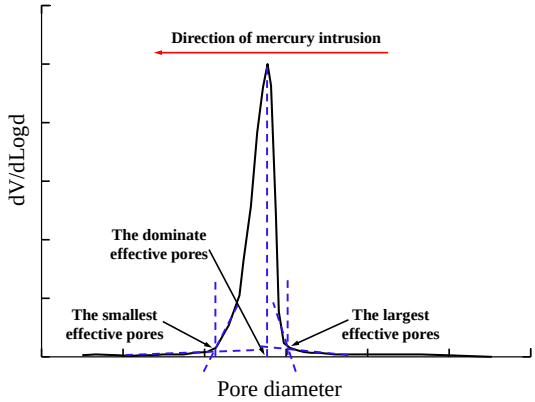

Fig. 5 Definitions of the largest effective pore and the smallest pore diameters

Table 1 The parameters obtained by PSDs for complete-intense weathering mudstone

PSD at 0 MPa	d_{max} (nm)	1000
	Applying pressure (psi)	241
	AEV (kPa)	245
PSD at 38 MPa	d_{min} (nm)	7
	Applying pressure (psi)	25000
	RV (kPa)	34930
	Calculated w_r at RV (%)	3

Fig. 4 shows the comparison between the measured SWRC and the prediction calculated by PSD of MIP test for undisturbed complete-intense weathering mudstone (Niu *et al.* 2019), Pearl clay (Gao and Sun 2017) and lateritic clay (Sun *et al.* 2016). As illustrated in Fig. 4(a), as the complete-intense weathering mudstone is a deformable clay, the predictions calculated by the PSDs under different suctions are different. In total suction range, the curve calculated by the PSD under 0 MPa suction is more successful than the one by PSD under 38 MPa suction. But, the prediction by PSD under 0 MPa suction can not match the test data well in lower suction range. The PSD changes significantly during the SWRC test, and this change can cause the discrepancies between predicted and measured curves (Simms and Yanful 2002). Thus, the prediction can not match the experiments well only by using one PSD for a deformable clay. Fig. 4(b) shows the experiments and prediction by PSD for Pearl clay (a silt). It can be seen that the calculation by PSD is in a better agreement with experimental data in medium and high suction ranges. Fig. 1(c) shows the measured and predicted SWRCs obtained by PSD for lateritic clay. It can be seen that compacted lateritic clay has bimodal SWRC and the prediction can also describe the bimodal shape. After exploring these experiments and predictions by PSD, the calculated curves

are in good agreement with experimental data in medium and high suction ranges, but can not match the test data reasonably well in lower suction range. Based on the comparison the measurements and predictions obtained by PSDs, the curve shapes of predictions and measurements are the same. Although the predicted curves are not reasonable in lower suction range, the calculated suctions at all turning points are the same with the measured suction in SWRC. In other words, the suctions at AEV and RV predicted by PSD are in good agreement with experimental SWRC.

3. The relationship between PSD and SWRC

Water retention behavior in soils is highly dependent on the individual pores. Thus, PSD is more commonly used to explain the soil water retention behavior (Sun *et al.* 2016). And PSD can be obtained by MIP test, scanning electron microscope (SEM) and nuclear magnetic resonance (NMR). The pore structure of soils can be characterized unimodal, bimodal and multimodal PSD. Generally, there are two pivotal points in typical SWRC. The first point is AEV where the pores in soils start to desaturate. The second point is RV where the water in soils becomes significantly more difficult to remove (Fredlund *et al.* 2011). According to BCC model and Young-Laplace equation, AEV is the suction, where the largest effective pores start draining and RV involves the suction, where the smallest effective pores start draining (Niu *et al.* 2020).

The AEV of SWRC is corresponding to the largest effective pore and the RV is in a good agreement with the smallest effective pore. As illustrated in Fig. 5, the largest effective pore and the smallest pore can be determined by following this procedure: Determine the point of the maximum slope on the right side of the peak shape and draw the tangent line through this point. Then draw another tangent line through the point where the curve starts to drop linearly in the large pore diameter range. The intersection of the two tangent lines is the largest effective pore diameter. In the same way, the smallest pore diameter can be determined the left side of the peak shape. Fig. 6 shows the relationship between SWRC and PSD for three materials. Based on Eqs (1) and (2), there is a specific relationship between the pore diameter and the suction in SWRC test. Thus, SWRC can be plotted the relationship between water content and pore distribution behavior. Fig. 6(a) shows the dependency of SWRC on PSD for undisturbed complete-intense weathering mudstone. As shown in Fig. 4(a), the AEV of undisturbed complete-intense weathering mudstone is about 250 kPa and the suction of RV is about 3.4×10^4 kPa. As illustrated in Fig. 6(a), using the mentioned procedure for determining the largest and smallest effective pore diameters, the largest effective pore diameter controlling AEV is about 1000 nm, and the smallest effective pore diameter controlling RV is about 7 nm. According to Eq. (3), the suctions at AEV and RV calculated by PSD are about 245 kPa and 3.5×10^4 kPa. The key parameters in SWRC and PSD for complete-intense weathering mudstone are illustrated in Table 1. It can be seen that the suctions at AEV and RV are in a good

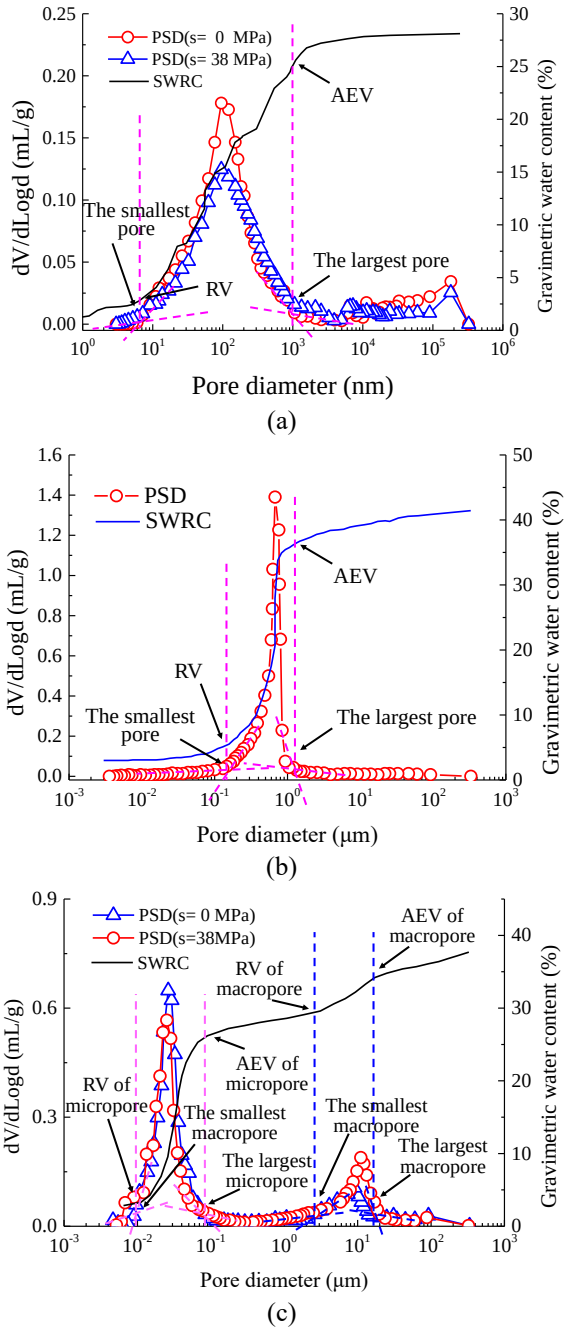

Fig. 6 The relationship between SWRC and PSD: (a) for undisturbed complete-intense weathering mudstone (modified from Niu *et al.* 2019), (b) for reconstituted Pearl clay (modified from Gao and Sun 2017) and (c) for compacted lateritic clay (modified from Sun *et al.* 2016)

agreement with the measured values in SWRC test. This further proves the correctness of the mentioned relationship between PSD and SWRC.

As shown in Fig. 4(b), the AEV of reconstituted Pearl clay is about 220 kPa and the suction of RV is about 1.7×10^3 kPa by graphic method. As illustrated in Fig. 6(b), for Pearl clay, the largest effective pore diameter can also be determined as about 1150 nm, and the smallest effective pore diameter controlling RV is about 150 nm. According to Eq. (3), the suctions at AEV and RV calculated by PSD are

Table 2 The parameters obtained by PSD for Pearl clay

PSD at 0 MPa	d_{max} (nm)	1157
	Applying pressure (psi)	161
	AEV (kPa)	200
	d_{min} (nm)	151
	Applying pressure (psi)	1196
	RV (kPa)	1615
	Calculated w_r at RC (%)	3

Table 3 The parameters obtained by PSDs for Lateritic clay

PSD at 0 MPa	Peak 1	d_{max} of Peak 1 (nm)	12508
		Applying pressure at d_{max} of Peak 1 (psi)	14.46
		Suction at d_{max} of Peak 1 (kPa)	19.5
		d_{min} of Peak 1 (nm)	2110
		Applying pressure at d_{min} of Peak 1 (psi)	85.6
		Suction at d_{min} of Peak 1 (kPa)	116
PSD at 38 MPa	Peak 2	d_{max} of Peak 2 (nm)	95.4
		Applying pressure at d_{max} of Peak 2 (psi)	1895
		Suction at d_{max} of Peak 2 (kPa)	2600
		Calculated w_r at d_{min} of Peak 2 (%)	26
		d_{min} of Peak 2 (nm)	7.2
		Applying pressure at d_{min} of Peak 2 (psi)	24985
		Suction at d_{min} of Peak 2 (kPa)	33700
		Calculated w_r at d_{min} of Peak 2 (%)	3.5

about 200 kPa and 1.6×10^3 kPa. Thus, the suctions at AEV and RV calculated by PSD can match the values in SWRC by graphic method. The key parameters in SWRC and PSD for reconstituted Pearl clay are illustrated in Table 2.

As illustrated in Fig. 4(c), there are two AEVs and RVs inter-aggregate pores and intra-aggregate respectively for lateritic clay. The first AEV is governed by the largest effective pores of inter-aggregate pores (peak 1) and the second AEV is governed by the largest effective pores of intra-aggregate pores (peak 2), as illustrated in Fig. 6(c). Similarly, the first RV is governed by the smallest effective pores of inter-aggregate pores and the second RV is governed by the smallest effective pores of intra-aggregate pores. As illustrated in Fig. 4(c), the AEV and RV of lateritic clay can be determined in SWRC by graphic method. The largest effective pore diameters and smallest pore diameters of inter-aggregate pores and intra-aggregate pores can also be determined in Fig. 6(c). The key parameters in SWRC and PSD are shown in Table 3. It can be seen that the suctions at AEVs and RVs determined by graphic method are in good agreement with the values calculated by PSD.

4. The relationship between SSC and SWRC

SSC of slurry can be divided into three stages: normal shrinkage, residual shrinkage and zero shrinkage (Sun and Cui 2017). In normal shrinkage stage, the change ratio of water content is same as the reduce ratio of void ratio during drying. In residual shrinkage stage, the reduce ratio of void ratio is lower than the ratio of water content during further drying. In zero shrinkage stage, water content continues reducing during drying, whereas void ratio nearly unchanged. The separating point between SSC and consolidation curve of saturated soil is corresponding to AEV. And the turning point, where void ratio nearly unchanged is can be called shrinkage limit. Fig. 7 shows the relationship between SWRC and SSC for reconstituted

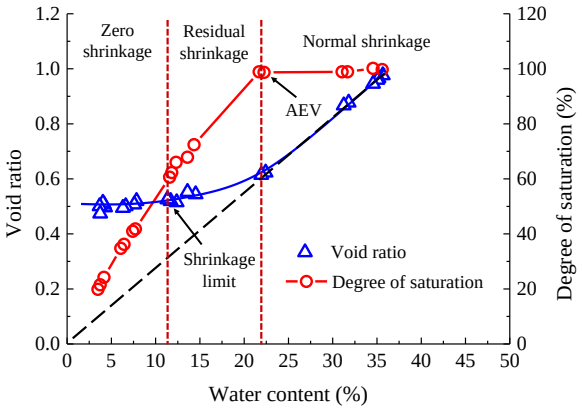

Fig. 7 The relationship between SWRC and SSC for reconstituted Jossigny silt (after Sun and Cui 2017)

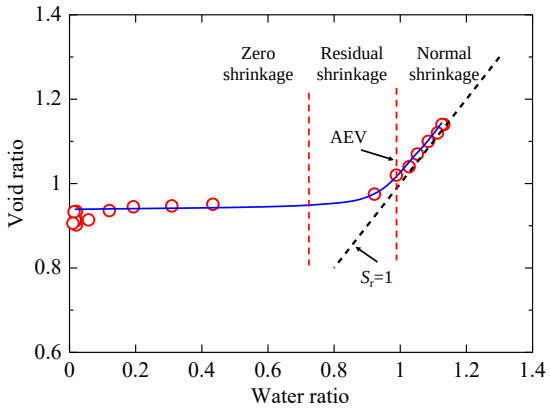

Fig. 8 SSC for reconstituted Pearl clay (after Gao and Sun 2017)

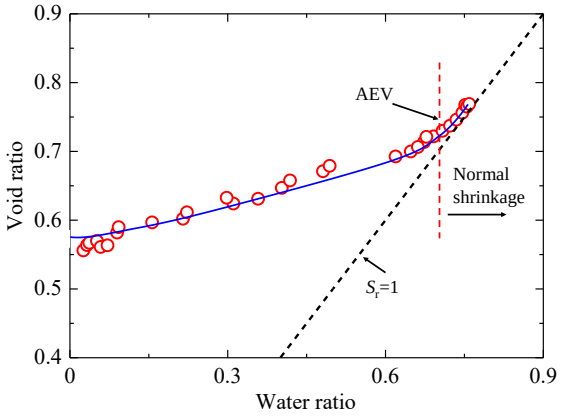

Fig. 9 SSC for undisturbed complete-intense weathering mudstone (after Niu *et al.* 2019)

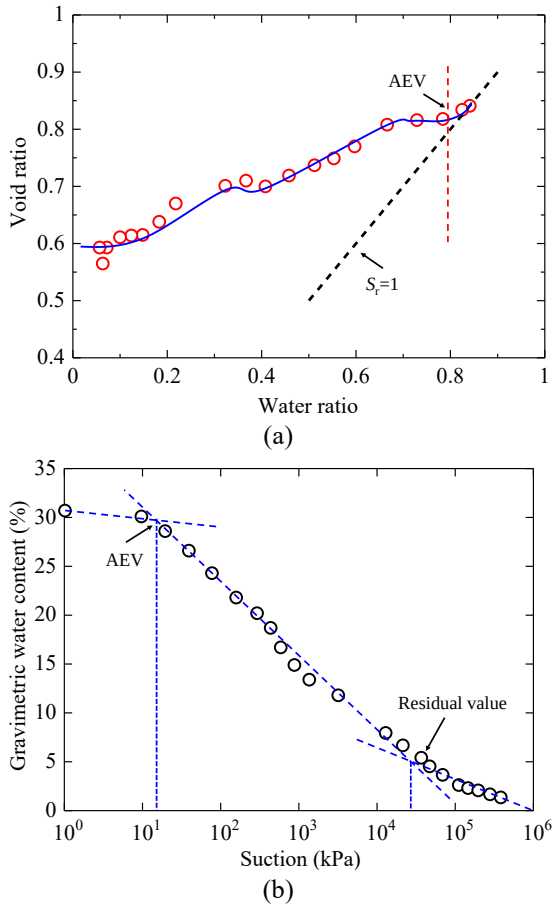

Fig. 10 (a) SSC for a compacted weakly expansive soil and (b) SWRC for a compacted weakly expansive soil (after Zhang *et al.* 2020)

Jossigny silt (Sun and Cui 2017). It can be confirmed that the separating point between consolidation curve of saturated soil and SSC is the AEV in SWRC.

Fig. 8 shows the SSC for reconstituted Pearl clay. It can be seen that the water ratio, where SCC starts separate from consolidation curve of saturated soil is about 0.98. As illustrated in Fig. 4(b), it can be seen that the AEV of reconstituted Pearl clay by graphic method is about 200 kPa and the water ratio correspondingly is about 0.97. The separating point between SCC and consolidation curve of saturated soil is in agreement with AEV in SWRC. Fig. 9 shows the SSC for undisturbed complete-intense weathering mudstone (Niu *et al.* 2019). The water ratio in separating point between SCC and consolidation curve of saturated soil is about 0.7. As illustrated in Fig. 4(a), the AEV for undisturbed complete-intense weathering mudstone can be determined as 250 kPa by graphic method and the water ratio correspondingly is about 0.7. Thus, the water ratio at AEV is corresponding to the value where the separating point between SCC and consolidation curve of saturated soil. And Fig. 10 shows the SSC and SWRC for a compacted weakly expansive soil (Zhang *et al.* 2020). The water ratio in separating point between SCC and consolidation curve of saturated soil is about 0.79. And the water ratio at AEV in SWRC by graphic method is about 0.8. Thus, the conclusion that the separating point between SCC and consolidation curve of saturated soil is corresponding to AEV in SWRC can be accepted. These experimental data report that the separating point between SSC and consolidation curve of saturated soil in shrinkage test is corresponding to AEV in SWRC test. But the gravimetric water content at RV can not be determined from SSC.

5. Determination of SWRC variables from PSD and SSC

Some SWRC variables such as AEV, the water content at AEV, the slope at the inflection point, RV and the water content at RV are the key points in SWRC. These key variables are commonly used to describe the water retention behavior (Zhai and Rahardjo 2012), shear strength (Gao *et al.* 2020), compressive stiff (Zhang *et al.* 2018), water evaporation (Song and Cui 2020) and permeability (Shao *et al.* 2017). Generally, these SWRC variables can be defined by graphical method. In the conventional graphical method, the experiments need to be measured firstly. Thus, this method is time consuming for measuring the SWRC data.

As investigated in sections 2 and 3, the AEV in SWRC can be determined by PSD of MIP test. For unimodal structural soil, the largest effective pores govern AEV. For bimodal structural soil, the largest effective pores of inter-aggregates govern AEV of macro-pores and the largest effective pores of intra-aggregates govern AEV of micro-pores. However, the gravimetric water content calculated by PSD of MIP test at AEV is not in good agreement with the measured gravimetric water content (see Figs. 4(a), 4(b) and 4(c)). As illustrated in section 4, the separating point between consolidation curve of saturated soil and SSC is corresponding to the AEV in SWRC and the gravimetric water content at separating point is in good agreement with the measured water content. Thus, the water content and suction at air entrance condition can be defined by PSD and SSC.

As illustrated in sections 2 and 3, the RV can also be determined by PSD of MIP test. For unimodal structural soil, the smallest effective pores govern RV. For bimodal structural soil, the smallest effective pores of inter-aggregates govern RV of macro-pores and the smallest effective pores of intra-aggregates govern RV of micro-pores. In addition, based on the investigation of experiments, the gravimetric water content at RV obtained by PSD is in good agreement with the measured water content in SWRC (see Figs. 4(a), 4(b) and 4(c)). Thus, the gravimetric water content at RV can be calculated by PSD. Based on SSC and PSD, the SWRC variables such as AEV, the gravimetric water content at AEV, the slope at the inflection point, RV and the gravimetric water content at RV for unimodal and bimodal structural soils can be defined. It should be noted that the gravimetric water content and suction at RV need to be calculated by the PSD under a high suction.

6. A simplified method to estimate unimodal SWRC

Generally, for unimodal SWRC (Figs. 4(a) and (b)), the

two key points (AEV and RV) can split the curve into boundary effect zone, transition zone and residual zone (Pham and Fedlund 2008). And each zone can be described by linear expression respectively:

$$\begin{aligned} w_{\mathrm{I}} &= w_{\mathrm{s}} - s_{\mathrm{I}}\log(\psi) && \psi \le \psi_{\mathrm{AEV}} \\ w_{\mathrm{II}} &= w_{\mathrm{AEV}} - s_{\mathrm{II}}\log(\frac{\psi}{\psi_{\mathrm{AEV}}}) && \psi_{\mathrm{AEV}} \le \psi \le \psi_{\mathrm{RV}} \\ w_{\mathrm{III}} &= s_{\mathrm{III}}\log(\frac{10^6}{\psi}) && \psi \ge \psi_{\mathrm{RV}} \end{aligned} \quad (7)$$

where w_{I},w_{II},w_{III} are gravimetric water contents in three portions; s_{I}, s_{II} and s_{III} are the slopes of the straight lines in three portions; ψ is suction; w_{AEV} is the gravimetric water content at AEV; w_{s} is gravimetric water content od saturated soil; ψ_{AEV} is AEV. Although the method is simple, the gravimetric water contents at AEV and RV and the three slopes are difficult to determine. Moreover, it is difficult to determine the suctions at AEV and RV.

The start point (saturated condition) of SWRC can be considered as the suction is 0.1 kPa and the gravimetric water content is the water content of saturated soil. The end point ("zero water storage") can be considered as the suction is 10^6 kPa and gravimetric water content is 0. If the suctions and gravimetric water contents at AEV and RV can be also determined, the three linear segments of typical SWRC in total suction range can be written as follow (Wijaya and Leong 2016, Niu *et al.* 2020):

$$\begin{aligned} w &= -\frac{w_{\mathrm{s}}-w_{\mathrm{AEV}}}{\log(\frac{\psi_{\mathrm{AEV}}}{0.1})}\log\psi + w_{\mathrm{s}} && \psi \le \psi_{\mathrm{AEV}} \\ w &= -\frac{w_{\mathrm{AEV}}-w_{\mathrm{RV}}}{\log(\frac{\psi_{\mathrm{RV}}}{\psi_{\mathrm{AEV}}})}\log\psi + w_{\mathrm{AEV}} + \frac{w_{\mathrm{AEV}}-w_{\mathrm{RV}}}{\log(\frac{\psi_{\mathrm{RV}}}{\psi_{\mathrm{AEV}}})}\psi_{\mathrm{AEV}} && \psi_{\mathrm{AEV}} \le \psi \le \psi_{\mathrm{RV}} \\ w &= -\frac{w_{\mathrm{RV}}}{\log(\frac{10^6}{\psi_{RV}})}\log\psi + w_{\mathrm{RV}} + \frac{w_{\mathrm{RV}}}{\log(\frac{10^6}{\psi_{RV}})}\psi_{RV} && \psi \ge \psi_{\mathrm{RV}} \end{aligned} \quad (8)$$

where w_{AEV} and w_{RV} are the gravimetric water contents in AEV and RV respectively; Ψ_{AEV} and Ψ_{RV} are the matric suctions in AEV and RV respectively.

As illustrated in section 3, the pores where mercury starts to intrude obviously are the largest effective pores, which govern the AEV. And the smallest effective pores governing the RV, where it starts significantly more difficult to intrude mercury as pressure increasing. If the largest and smallest effective pore diameters can be determined, then the suctions and gravimetric water contents at AEV and RV can be obtained respectively by the Eqs. (2), (3), (4), (5) and (6). It can be seen in Section 2 and 3, although the predicted gravimetric water content at AEV could not match the measured results quilt well, the AEV calculated by the largest pore diameter determined by MIP test is closely approximate to AEV obtained in SWRC test. The calculated gravimetric water content and suction by PSD at RV are in good agreement with the values in SWRC obtained by graphic method. As illustrated in Section 4, the separating point between consolidation curve of saturated soil and SSC is the corresponding to AEV in SWRC. And the gravimetric water content in separating point is in good agreement with the value in SWRC obtained by graphic method. Thus, the variables of SWRC can be determined by PSD and SSC.

Table 4 The variables of SWRC for complete-intense weathering mudstone and Pearl clay

Soil	Variables of SWRC	Value	Obtained method
Complete-intense weathering mudstone	AEV (kPa)	245	PSD (s=0 kPa)
	w at AEV	36.7	SSC
	Suction at RV (kPa)	3.5×10^4	PSD (s=38 kPa)
	w at RV (%)	3	PSD (s=38 kPa)
Pearl clay	AEV (kPa)	200	PSD (s=0 kPa)
	w at AEV	26.3	SSC
	Suction at RV (kPa)	1600	PSD (s=0 kPa)
	w at RV	3	PSD (s=0 kPa)

There are four parameters which can be determined by the PSDs from MIP tests and SSC in equations for unimodal SWRC. Moreover, no curve-fitting procedures are necessary in the proposed method to construct SWRC. And the parameters in proposed equations have explicit physical meanings respectively.

7. Verification of proposed equations using experimental data from the literature

The validity of proposed method to construct SWRC is demonstrated by comparing predictions with experimental data. In order to demonstrate the advantages of the proposed equation, two materials (undisturbed complete-intense weathering mudstone (liquid limit = 52.6%, plasticity index = 26.7) (Niu *et al.* 2019) and reconstituted Pearl clay (a silt, liquid limit = 43%, plasticity index = 26%) (Gao and Sun 2017)) were used.

As illustrated in Fig. 6(a), the largest effective pore diameter governing AEV can be determined by the PSD under 0 kPa suction condition, and the AEV can be obtained by Eqs. (1)-(3). And the gravimetric water content at AEV can be determined by SSC (see in Fig. 9). The gravimetric water content of the separating point between consolidation curve of saturated soil and SSC is about 26.3% as shown in Fig. 9. The smallest effective pore diameter governing RV can be determined by the PSD under 38 MPa suction

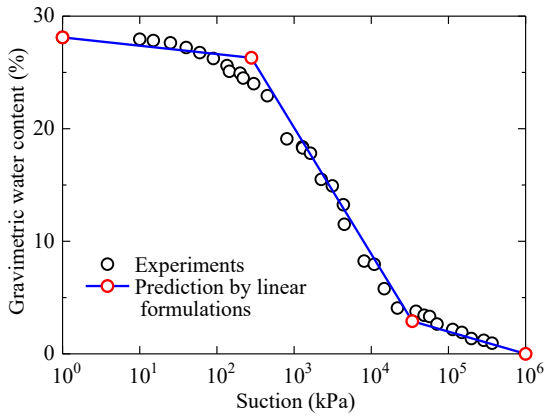

Fig. 11 Comparison of predicted and measured SWRCs for undisturbed complete-intense weathering mudstone

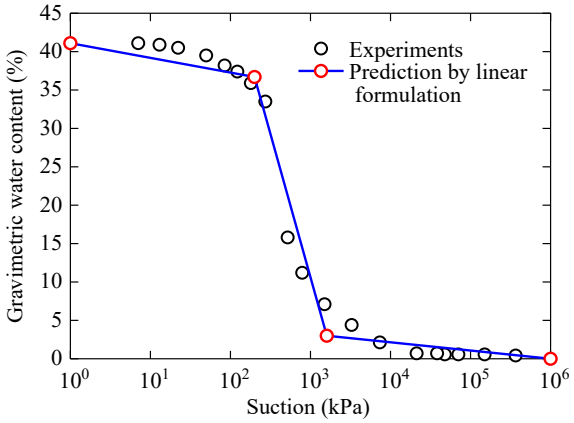

Fig. 12 Comparison of predicted and measured SWRCs for reconstituted Pearl clay

condition (see in Fig. 6(a)), then the suction and gravimetric water content at RV can be obtained by Eqs. (1)-(3) and Eqs. (4)-(6) respectively. At last, these key variables in SWRC obtained by PSDs for complete-intense weathering mudstone are determined. These variables of SWRC obtained by PSDs and SSC for complete-intense weathering mudstone are illustrated in Table 4. Then substitution of the parameters into Eq. (8) leads to the SWRC of undisturbed complete-intense weathering mudstone. Fig. 11 shows the experiments and calculation by PSD and SSC. As illustrated in Fig. 11, the predicted SWRC obtained by the proposed method can match the experimental data (void ratio e=0.77) well.

According to the procedure described in section 3, the largest effective pore diameter and smallest pore diameter for reconstituted Pearl clay can be determined by the PSD (see in Fig. 6(b)). Then the suctions at AEV and RV can be obtained by Eqs. (1)-(3) and the gravimetric water content in RV can be obtained by Eqs. (4)-(6). The gravimetric water content of the separating point between consolidation curve of saturated soil and SSC of reconstituted Pearl clay is about 36.7% as shown in Fig. 8. These variables of SWRC obtained by PSD and SSC for reconstituted Pearl clay are illustrated in Table 4. SWRC can be obtained by substituting these parameters determined from PSD into Eq. (8). Fig. 12 shows the measured and predicted results of the SWRC for reconstituted Pearl clay in the main drying (e=1.10). It can be seen that the prediction obtained by proposed equations is in good agreement with experimental data.

8. Conclusions

In order to determine SWRC variables directly without prior measured SWRC data, an insight into the relationship between SWRC, PSD and SSC is investigated. In unimodal PSD curve, the largest effective pores govern the AEV, and the smallest effective pores govern the RV. For bimodal SWRC, the AEV and RV of inter-aggregate are governed by the largest effective pores and smallest pores of inter-aggregate respectively respectively. Considering shrinkage, the AEV can be determined by the PSD of 0 suction. While the RV and gravimetric water content at RV can be determined by the PSD of a higher suction. In the combination of SSC and SWRC, the separating point between consolidation curve of saturated soil and SSC is corresponding to the AEV in SWRC and the gravimetric water content at separating point is in good agreement with the value at AEV in SWRC. Thus, these SWRC parameters can be defined directly by the PSD of MIP test and SSC without fitting process.

Unimodal SWRC can be discretized as three linear segments respectively through these key points, and each segment can be represented by linear formulation. The coordinate (suction and gravimetric water content) of each turning point can be determined by the PSD and SSC correspondingly. There are four parameters for unimodal SWRC and these parameters can be determined by PSDs and SSC. Each parameter in proposed equations has definitude physical meaning in proposed unimodal SWRC equations. The proposed method is verified by experimental SWRC data of silts and deformable clays. In addition, this method can construct the unimodal SWRC directly without fitting SWRC data process. It is however worth noting that the proposed equations are difficult to be substituted into constitutive modelling because of its discontinuity.

Acknowledgments

This research was funded by National Key Laboratory Funding of Independent Research Project (grant number S18406), National Natural Science Foundation of China (grant number 51479023), and National Natural Science Foundation of Liaoning (grant number 2019-ZD-0187).

References

An, N., Hemmati, S. and Cui, Y.J. (2017), "Numerical analysis of soil volumetric water content and temperature variations in an embankment due to soil-atmosphere interaction", *Comput. Geotech.*, **83**, 40-51. https://doi.org/10.1016/j.compgeo.2016.10.010.

An, N., Hemmati, S., Cui, Y.J. and Tang, C.S. (2018), "Numerical investigation of water evaporation from Fontainebleau sand in an environmental chamber", *Eng. Geol.*, **234**, 55-64. https://doi.org/10.1016/j.enggeo.2018.01.005.

Aung, K.K., Rahardjo, H., Leong, E.C. and Toll, D.G. (2001), *Relationship between Porosimetry Measurement and Soil-Water Characteristic Curve for an Unsaturated Residual Soil*, in *Unsaturated Soil Concepts and Their Application in Geotechnical Practice*, Springer, Dordrecht, Germany, 401-416.

Chin, K.B., Leong, E.C. and Rahardjo, H. (2010), "A simplified method to estimate the soil-water characteristic curve", *Can. Geotech. J.*, **47**(12), 1382-1400. https://doi.org/10.1139/T10-033.

Darde, B., Roux, J.N., Pereira, J.M., Dangla, P., Talandier, J., Vu, M.N. and Tang, A.M. (2020), "Investigating the hydromechanical behaviour of bentonite pellets by swelling pressure tests and discrete element modelling", *Acta Geotech.*, 1-18. https://doi.org/10.1007/s11440-020-01040-5.

Fredlund, D.G. (2019), "State of practice for use of the soil-water

characteristic curve (SWCC) in geotechnical engineering", *Can. Geotech. J.*, **56**(8), 1059-1069. https://doi.org/10.1139/cgj-2018-0434.

Fredlund, D.G., Sheng, D. and Zhao, J. (2011), "Estimation of soil suction from the soil-water characteristic curve", *Can. Geotech. J.*, **48**(2), 186-198. https://doi.org/10.1139/T10-060.

Gao, Y. and Sun, D.A. (2017), "Soil-water retention behavior of compacted soil with different densities over a wide suction range and its prediction", *Comput. Geotech.*, **91**, 17-26. https://doi.org/10.1016/j.compgeo.2017.06.016.

Gao, Y., Sun, D.A., Zhou, A. and Li, J. (2020), "Predicting shear strength of unsaturated soils over wide suction range", *Int. J. Geotech.*, **20**(2), 04019175. https://doi.org/10.1061/(ASCE)GM.1943-5622.0001555.

Niu, G., Shao, L., Sun, D. A. and Guo, X. (2020), "A simplified directly determination of soil-water retention curve from pore size distribution", *Geomech. Eng.*, **20**(5), 411-420. https://doi.org/10.12989/gae.2020.20.5.411

Niu, G., Sun, D.A., Shao, L. and Zeng, L. (2019), "The water retention behaviours and pore size distributions of undisturbed and remoulded complete-intense weathering mudstone", *Eur. J. Environ. Civ. Eng.*, 1-18. https://doi.org/10.1080/19648189.2019.1572544.

Or, D. and Tuller, M. (2002), "Cavitation during desaturation of porous media under tension", *Water Resour. Res.*, **38**(5), 1-4. https://doi.org/10.1029/2001WR000282.

Oren, A.H., Aksoy, Y.Y., Onal, O. and Demirkiran, H. (2018), "Correlating the hydraulic conductivities of GCLs with some properties of bentonites", *Geomech. Eng.*, **15**(5), 1091-1100. https://doi.org/10.12989/gae.2018.15.5.1091.

Pereira, J. M., Wong, H., Dubujet, P. and Dangla, P. (2005), "Adaptation of existing behaviour models to unsaturated states: Application to CJS model", *Int. J. Numer. Anal. Met.*, **29**(11), 1127-1155. https://doi.org/10.1002/nag.453.

Pham, H.Q. and Fredlund, D.G. (2008), "Equations for the entire soil-water characteristic curve of a volume change soil", *Can. Geotech. J.*, **45**(4), 443-453. https://doi.org/10.1139/T07-117.

Rahimi, A., Rahardjo, H. and Leong, E.C. (2015), "Effect of range of soil-water characteristic curve measurements on estimation of permeability function", *Eng. Geol.*, **185**, 96-104. https://doi.org/10.1016/j.enggeo.2014.11.017.

Romero Morales, E.E. (1999), "Characterisation and thermo-hydro-mechanical behaviour of unsaturated Boom clay: An experimental study", Ph.D. Dissertation, Polytechnic University of Catalonia, Barcelona, Spain.

Russell, A.R. (2014), "How water retention in fractal soils depends on particle and pore sizes, shapes, volumes and surface areas", *Géotechnique*, **64**(5), 379-390. https://doi.org/10.1680/geot.13.P.165.

Salager, S., Nuth, M., Ferrari, A. and Laloui, L. (2013), "Investigation into water retention behaviour of deformable soils", *Can. Geotech. J.*, **50**(2), 200-208. https://doi.org/10.1139/cgj-2011-0409.

Shao, L., Wen, T., Guo, X. and Sun, X. (2017), "A method for directly measuring the hydraulic conductivity of unsaturated soil", *Geotech. Test. J.*, **40**(6), 907-916. https://doi.org/10.1520/GTJ20160197.

Sheng, D., Sloan, S.W. and Gens, A. (2004), "A constitutive model for unsaturated soils: Thermomechanical and computational aspects", *Comput. Mech.*, **33**(6), 453-465. https://doi.org/10.1007/s00466-003-0545-x.

Simms, P.H. and Yanful, E.K. (2002), "Predicting soil-water characteristic curves of compacted plastic soils from measured pore-size distributions", *Géotechnique*, **52**(4), 269-278. https://doi.org/10.1680/geot.2002.52.4.269.

Song, W.K. and Chen, Y. (2020), "Modelling of evaporation from free water surface", *Geomech. Eng.*, **21**(3), 237-245. https://doi.org/10.12989/gae.2020.21.3.237.

Sun, D.A., You, G., Annan, Z. and Daichao, S. (2016), "Soil-water retention curves and microstructures of undisturbed and compacted Guilin lateritic clay", *B. Eng. Geol. Environ.*, **75**(2), 781-791. http://doi.org/10.1007/s10064-015-0765-2.

Sun, W.J. and Cui, Y.J. (2017), "Investigating the microstructure changes for silty soil during drying", *Géotechnique*, **68**(4), 370-373. https://doi.org/10.1680/jgeot.16.P.165.

Wang, Y., Cui, Y.J., Tang, A.M., Tang, C.S. and Benahmed, N. (2016), "Changes in thermal conductivity, suction and microstructure of a compacted lime-treated silty soil during curing", *Eng. Geol.*, **202**, 114-121. https://doi.org/10.1016/j.enggeo.2016.01.008.

Wijaya, M. and Leong, E.C. (2016), "Equation for unimodal and bimodal soil-water characteristic curves", *Soils Found.*, **56**(2), 291-300. https://doi.org/10.1016/j.sandf.2016.02.011.

Xu, Y. (2004), "Calculation of unsaturated hydraulic conductivity using a fractal model for the pore-size distribution", *Comput. Geotech.*, **31**(7), 549-557. https://doi.org/10.1016/j.compgeo.2004.07.003.

Zhai, Q. and Rahardjo, H. (2012), "Determination of soil-water characteristic curve variables", *Comput. Geotech.*,**42**, 37-43. https://doi.org/10.1016/j.compgeo.2011.11.010

Zhang, F., Cui, Y., Zeng, L., Robinet, J.C., Conil, N. and Talandier, J. (2018), "Effect of degree of saturation on the unconfined compressive strength of natural stiff clays with consideration of air entry value", *Eng. Geol.*, **237**, 140-148. https://doi.org/10.1016/j.enggeo.2018.02.013.

Zhang, J., Niu, G., Li, X. and Sun, D.A. (2020), "Hydro-mechanical behavior of expansive soils with different dry densities over a wide suction range", *Acta Geotech.*, **15**(1), 265-278. https://doi.org/10.1007/s11440-019-00874-y.

Zhang, X. and Lytton, R.L. (2012), "Modified state-surface approach to the study of unsaturated soil behavior. Part III: Modeling of coupled hydromechanical effect", *Can. Geotech. J.*, **49**(1), 98-120. https://doi.org/10.1139/t11-089.

Zhou, A.N, Huang, R. and Sheng, D.C. (2016), "Capillary water retention curve and shear strength of unsaturated soils" *Can. Geotech. J.*, **53**(6), 974-987. https://doi.org/10.1139/cgj-2015-0322.

IC